Available online at www.sciencedirect.com
SCIENCE DIRECT
ELSEVIER
Journal of the European Ceramic Society 26 (2006) 1761–1766
ECERS
www.elsevier.com/locate/jeurceramsoc

Effect of phase transition on the microwave dielectric properties of $BiNbO_4$

Eung Soo Kim *, Woong Choi

Department of Materials Engineering, Kyonggi University, 94-6 Yiei-dong, Youngtong-gu, Suwon, Kyonggi-do 443-760, Korea

Available online 17 October 2005

Abstract

$BiNbO_4$ specimens were transformed from the orthorhombic to triclinic phase at 1040 °C. The calculated intrinsic dielectric properties of the specimens were changed from $K = 42$, $Qf = 15700$ GHz in the orthorhombic phase to $K = 30$, $Qf = 8900$ GHz in the triclinic phase. The change of Qf value resulted from the increase of the dispersion parameter and modes for nonsymmetrical structure with the phase transition. *TCF* of the specimens decreased due to the increase of the octahedral distortion of $BiNbO_4$ with change from the orthorhombic to the triclinic phase. These results are due to the increase of bond valence of $BiNbO_4$ with the phase transition.
© 2005 Elsevier Ltd. All rights reserved.

Keywords: Powders-solid state reaction; X-ray methods; Dielectric properties; $BiNbO_4$; Functional applications

1. Introduction

Extensive studies have been carried out to develop low-temperature-cofired ceramics (LTCC) for microwave applications, due to the design and functional benefits realized upon the miniaturization of multilayer devices. [1–3] Bismuth-based dielectric ceramics are well known as low-firing materials and have been studied for multilayer capacitors.[4,5] Since Kagata et al.[6] reported the microwave dielectric properties of $BiNbO_4$ with sintering aids, various attempts have been undertaken to improve the microwave dielectric properties of $BiNbO_4$, such as the substitution of lanthanide for Bi,[7–9] the solid solutions of $Bi(Nb_{1-x}Ta_x)O_4$,[10] $Bi(Nb_{1-x}Sb_x)O_4$[11] and the addition of various sintering aids.[12,13] Also, the ABO_4 (A=Bi^{3+},Sb^{3+}, B=Nb^{5+},Ta^{5+},Sb^{5+}) compounds with stibiotantalite structure are known to exhibit multiple structural and dielectric phase transitions.

A fundamental relationship between the structural characteristics and the dielectric properties should be studied to control their dielectric properties. Therefore, it is necessary to study the intrinsic properties of $BiNbO_4$ with phase transition to predict and control the dielectric properties at microwave frequencies. Moreover, the far-infrared spectra measurement of dielectric materials has been known as a useful method to understand the dielectric constant and dielectric loss at microwave frequencies.[14]

In this study, the microwave dielectric properties of $BiNbO_4$ with phase transition were investigated as a function of sintering temperature. Far-infrared reflectivity spectra of the specimens were also investigated to evaluate the intrinsic dielectric loss with phase transition. The relationships between the microwave dielectric properties of the $BiNbO_4$ with phase transition and the bond valence,[15] the distortion of oxygen octahedron were discussed.

2. Experimental procedure

$BiNbO_4$ ceramics were prepared by the conventional mixed oxide method. The raw materials, Bi_2O_3 and Nb_2O_5, which had higher purity than 99.9%, were mixed in distilled water for 24 h with ZrO_2 balls, and this mixture was calcined twice at 750 °C for 3 h. The calcined powders were re-milled in water for 24 h. After the drying process, the powders were pressed into pellets at 1450 kg/cm^2, isostatically. These pressed specimens were sintered from 1000 to 1050 °C for 3 h, packed in an alumina crucible to inhibit the loss of Bi_2O_3.

Crystalline phases of the calcined powders and the sintered specimens were identified by X-ray diffraction pattern analysis (D/Max-3C, Rigaku, Japan) in the range 20–80° of 2θ using Cu kα radiation and the bulk densities of the sintered specimens were measured by the Archimedes method. The dielectric con-

* Corresponding author. Tel.: +82 31 249 9764; fax: +82 31 249 9775.
E-mail address: eskim@kyonggi.ac.kr (E.S. Kim).

0955-2219/$ – see front matter © 2005 Elsevier Ltd. All rights reserved.
doi:10.1016/j.jeurceramsoc.2005.09.003

stant (K) and the unloaded Q of the specimens at 7–9 GHz were measured by Hakki and Coleman's method,[16] and the temperature coefficient of resonant frequency (TCF) was measured in the temperature range from 20 to 80 °C by cavity method.[17]

The reflectivity spectra were measured, using Fourier-Transform infrared spectrometer (model DA-8.12, Bomen Inc., Toronto, Canada) from 50 to 4000 cm^{-1}; the surfaces of the samples were carefully ground and polished to a flatness of ~1 μm. The polished samples were set in a vacuum chamber evacuated to 0.3 torr (40 Pa), and the reflectivity spectra were obtained relative to the reflectivity of a gold mirror. The spectra were recorded at a resolution of 4 cm^{-1}. The incident angle of radiation was 7°.

From the individual bond lengths of oxygen octahedra reported by Subramanian and Calabrese for orthorhombic phase,[18] and Keve and Skapski for triclinic phase[19] for $BiNbO_4$, the octahedral distortion (Δ) was calculated from Eq. (1):[20]

$$\Delta = \frac{1}{6}\sum\left\{\frac{(R_i - \bar{R})}{\bar{R}}\right\}^2 \quad (1)$$

where R_i is the individual bond length, and R is average bond length of oxygen octahedron.

3. Results and discussion

Powder XRD patterns of $BiNbO_4$ specimens sintered at various temperatures are shown in Fig. 1. With the increase of sintering temperature up to 1030 °C for 3 h, the single orthorhombic $BiNbO_4$ phase was detected; however, the phase transition from orthorhombic to triclinic phase was observed for the specimens sintered at 1040 °C for 3 h, and the single triclinic $BiNbO_4$ phase was detected for further increase of sintering temperature and time. From the ICP data, the ratios of Bi to Nb were not changed with sintering temperature remarkably. Therefore, there was no severe volatilization of Bi through the phase transition. Even though there is a difference of phase transition temperature, these results are agreed with the report that $BiNbO_4$ has an orthorhombic $SbTaO_4$-type crystal structure below 1020 °C[18] and will transform to triclinic phase at higher temperatures.[19]

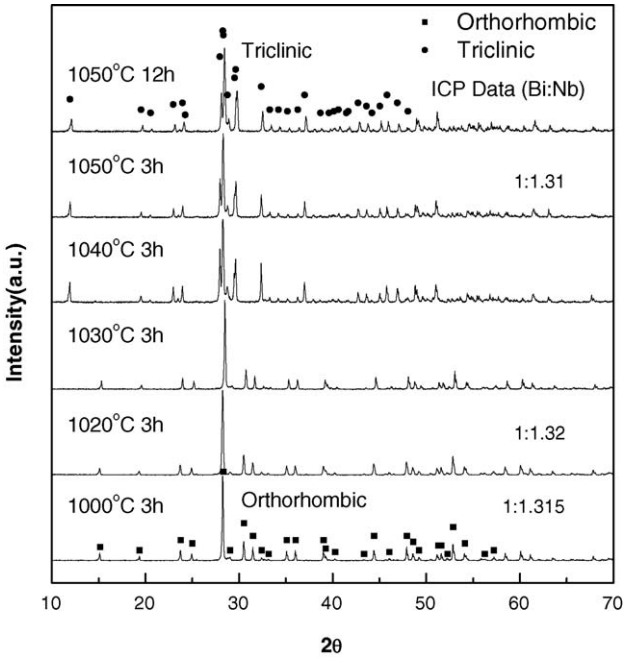

Fig. 1. X-ray diffraction patterns of $BiNbO_4$ specimens sintered at various temperatures.

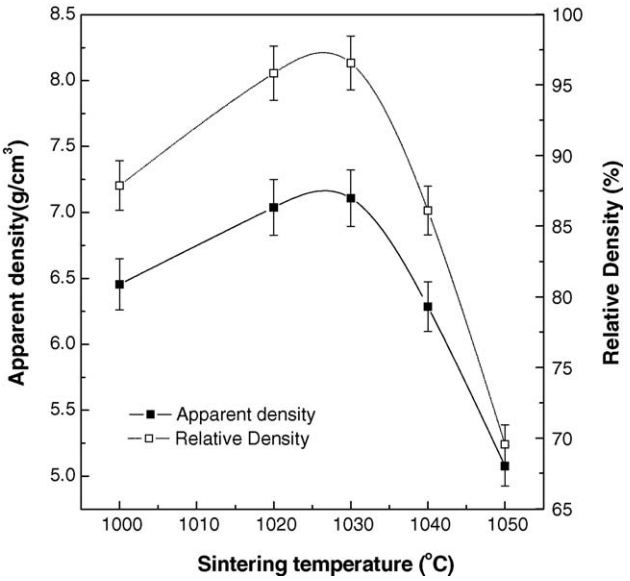

Fig. 2. Density of $BiNbO_4$ specimens sintered at various temperatures for 3 h.

Fig. 2 shows the density of the specimens as a function of sintering temperature. The density of the specimens increased with the sintering temperature up to 1030 °C and then decreased drastically for the specimens sintered at higher temperature than 1030 °C. These results were due to the lower sinterability of triclinic phase than that of orthorhombic $BiNbO_4$ phase.

Dielectric constant (K) and Qf value of the $BiNbO_4$ at microwave frequencies are shown in Fig. 3. With the increase of sintering temperature, K and Qf value of the specimens increased with sintering temperature up to 1030 and 1020 °C, respectively, and then decreased remarkably. However, $BiNbO_4$ was transformed from orthorhombic phase to triclinic phase at 1040 °C, and the density of the specimens was increased up to the sintering temperature of 1030 °C, as confirmed in Figs. 1 and 2. Because there was no evidence of discontinuous grain growth within the detection limits of SEM and EDS, the sudden drop in Q before maximum density has been reached could be attributed to the effect of secondary phase, and further investigations are undertaken to confirm the secondary phase. The measured K and Qf value at microwave frequencies included the intrinsic factors, such as crystal structure, lattice vibrations as well as extrinsic factors, such as impurity, density and the secondary phase.[21] Discrepancies between the microwave dielectric properties, especially Qf value ($Q \approx 1/\tan\delta$) with sintering temperature, and the phase transition temperature could also be explained by the

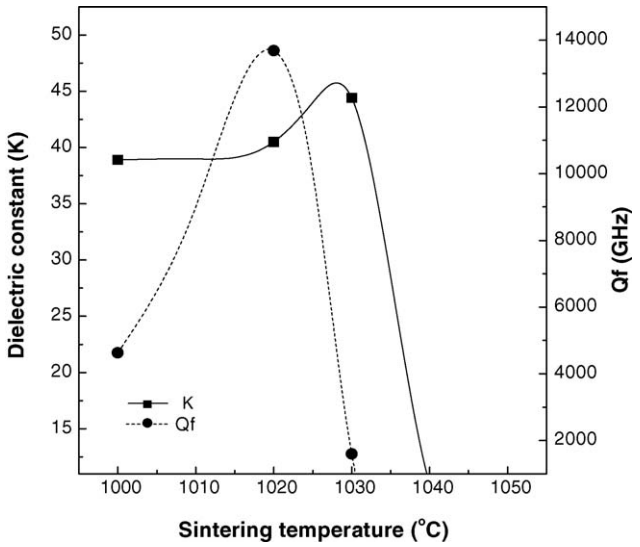

Fig. 3. Dielectric constant (K) and Qf value of $BiNbO_4$ specimens sintered at various temperatures for 3 h.

contribution of intrinsic factors to the microwave dielectric properties.

To clarify the intrinsic properties of $BiNbO_4$ specimens sintered from 1020 to 1040 °C, the far-infrared reflectivity spectra were obtained as shown in Fig. 4 and transformed to dielectric data by the Kramers–Kronig analysis.[22] Also, the classical oscillator model that leads to physically acceptable values outside the measured range was performed for these spectra. According to the classical oscillator model, the complex dielectric function can be expressed by Eq. (2)

$$\varepsilon^*(\omega) = \varepsilon_\infty + \sum_{j=1}^{n} \frac{S_j}{{\omega_j}^2 - \omega^2 + i\omega\gamma_j} \tag{2}$$

where $\varepsilon^*(\omega)$ is the complex dielectric function; n the number of transverse phonon modes: S_j, ω_j, and γ_j are the strength, phonon mode frequency and damping constant of the j_{th} mode, respectively, and ε_∞ is the dielectric constant caused by the electronic polarization at higher frequencies. The dielectric constant and loss tangent can be estimated under the condition of $\omega \ll \omega_j$:

$$\varepsilon'(\omega) = \varepsilon_\infty + \sum_j \Delta\varepsilon'_j \tag{3}$$

$$\tan\delta = \frac{\varepsilon''}{\varepsilon'} = \frac{\sum_j \Delta\varepsilon'(\gamma_J{}^{\omega})\omega_J^2}{\varepsilon_\infty + \sum_j \Delta\varepsilon'} \tag{4}$$

where $\Delta\varepsilon'_J = S_j/\omega'_J$

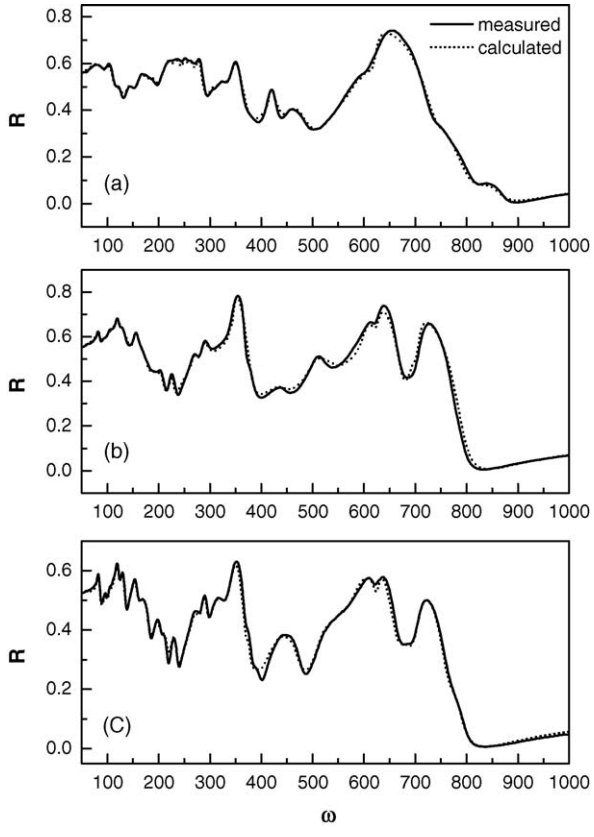

Fig. 4. Infrared reflectivity spectra of the dielectric function for $BiNbO_4$ sintered at various temperatures for 3 h: (a) 1020 °C, (b) 1030 °C and (c) 1040 °C.

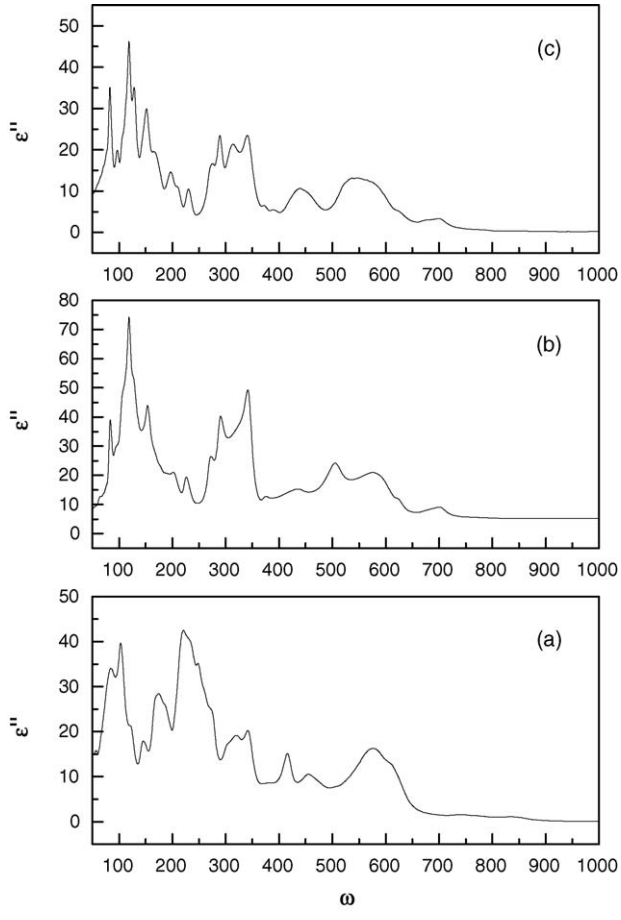

Fig. 5. Imaginary part of the dielectric function for $BiNbO_4$ specimens sintered at various temperatures for 3 h: (a) 1020 °C, (b) 1030 °C and (c) 1040 °C.

Table 1
Dispersion parameters of $BiNbO_4$ specimens obtained from the best fit to the reflectivity data

j	1020 °C				1030 °C				1040 °C			
	ω_j	γ	$\Delta\varepsilon'_j$	$\tan\delta$ ($\times10^4$)	ω_j	γ	$\Delta\varepsilon'_j$	$\tan\delta$ ($\times10^4$)	ω_j	γ	$\Delta\varepsilon'_j$	$\tan\delta$ ($\times10^4$)
1	83.5	32.3	10.0	2.75534	66.5	50.7	1.0	1.87654	71.53	50.682	9.01	6.76508
2	103.9	15.7	3.0	0.28396	83.5	6.6	1.8	0.11113	82.97	6.511	1.76	0.12367
3	123.0	20.1	1.0	0.07473	93.9	27.1	1.9	0.64710	96.48	5.466	0.53	0.01944
4	116.0	78.5	3.0	1.38155	105.4	17.8	1.4	0.26312	106.05	8.152	0.66	0.03541
5	143.7	8.6	0.3	0.00969	111.3	20.2	2.4	0.33322	112.22	8.543	0.45	0.02277
6	151.5	26.7	1.0	0.02522	118.6	9.7	2.7	0.14280	118.50	8.816	2.43	0.11348
7	166.4	7.8	0.4	0.00602	127.0	18.1	1.1	0.10749	128.70	9.875	1.71	0.07592
8	174.0	14.0	0.9	0.02125	129.5	23.1	1.9	0.21889	150.49	18.549	2.88	0.17526
9	187.9	25.0	2.1	0.08498	140.5	66.8	6.9	2.05532	170.19	20.347	1.51	0.07497
10	217.9	21.5	2.9	0.06791	153.8	9.8	1.0	0.02283	196.58	18.188	0.85	0.03044
11	234.5	21.9	2.2	0.04338	166.6	34.2	2.0	0.12863	211.23	15.730	0.40	0.01213
12	249.4	11.6	0.7	0.00465	191.1	16.1	0.3	0.00629	272.57	18.891	0.70	0.01472
13	261.0	18.7	1.1	0.01292	203.4	15.9	0.5	0.01155	288.80	12.729	0.66	0.00746
14	274.8	13.6	0.6	0.00447	226.4	9.2	0.3	0.00466	310.22	23.471	0.97	0.01763
15	304.8	33.8	1.2	0.02328	269.6	8.0	0.2	0.00170	342.95	20.055	0.81	0.01024
16	320.3	20.0	0.4	0.00341	274.5	11.3	0.2	0.00180	373.47	8.683	0.03	0.00014
17	331.0	25.0	0.4	0.00338	289.7	12.5	0.6	0.00590	390.02	22.413	0.05	0.00161
18	343.6	21.0	0.7	0.00391	298.4	38.6	2.0	0.05913	333.34	26.842	0.63	0.01137
19	374.8	110.2	0.3	0.02234	317.5	27.6	0.9	0.01599	320.23	16.430	0.25	0.00250
20	395.0	100.0	0.3	0.00821	329.1	20.2	0.7	0.00836	229.97	13.352	0.40	0.00897
21	410.0	60.9	0.7	0.01153	338.2	11.7	0.6	0.00322	436.21	62.575	1.19	0.03160
22	417.3	12.9	0.2	0.00083	346.1	9.6	0.9	0.00309	459.55	35.426	0.12	0.00183
23	468.9	36.6	0.2	0.00189	373.1	158.1	0.2	0.12747	523.07	33.990	0.35	0.00321
24	454.6	30.1	0.2	0.00146	405.5	67.5	0.4	0.01274	545.62	47.615	0.54	0.00636
25	475.5	126.7	0.7	0.04628	434.1	62.8	0.7	0.01681	580.01	62.535	1.07	0.01329
26	560.0	78.3	1.3	0.03679	474.1	62.0	0.3	0.00483	627.81	13.381	0.03	0.00004
27	580.4	35.4	0.3	0.00178	504.6	47.0	1.0	0.01407	674.93	34.952	0.06	0.00027
28	601.3	40.4	0.4	0.00242	532.5	75.2	0.9	0.02183	700.77	37.661	0.11	0.00065
29	621.2	18.3	0.2	0.00052	580.4	38.4	0.3	0.00245	704.38	20.535	0.01	0.00002
30	749.8	62.1	0.4	0.00063	597.4	32.5	0.5	0.00192	771.32	32.225	0.01	0.00003
31	772.6	90.6	0.0	0.00064	562.6	41.8	0.3	0.00316				
32	837.6	68.4	0.1	0.00047	621.6	12.8	0.0	0.00005				
33					627.2	15.0	0.1	0.00006				
34					690.2	33.4	0.2	0.00014				
35					704.8	13.3	0.0	0.00003				
36					730.6	16.2	1.9	0.00011				

The infrared reflectivity has been fitted with the aid of Eqs. (2) and (5):

$$R = \left| \frac{\sqrt{\varepsilon' - 1}}{\sqrt{\varepsilon' + 1}} \right|^2 \tag{5}$$

where, R is the reflectivity.

The calculated reflectivity spectra were well fitted with the measured ones, as shown in Fig. 4. The reflectivity spectrum of the specimens sintered at 1030 °C was similar to that of the specimens sintered at 1040 °C, even though the XRD pattern of the specimens sintered at 1030 °C was detected as the orthorhombic phase. From these reflectivity spectra, a real and an imaginary part of the complex dielectric function could be obtained.

Fig. 5 shows the imaginary part of the complex dielectric function for the $BiNbO_4$ specimens sintered from 1020 to 1040 °C. The spectra of the specimen sintered at 1020 and 1040 °C were fitted by 32 and 30 phonon modes, respectively, however, that of the specimen sintered at 1030 °C was well fitted by 36 phonon modes, as shown in Table 1. These results are due to the appearance of the degenerative modes for the increase of nonsymmetry in crystal structure. The dispersion parameters of the specimens in Table 1 were determined by the Kramers–Kronig analysis and classical oscillator model.

As shown in Table 2, the calculated dielectric constants of the specimens sintered at 1020 and 1030 °C agreed well with the measured values; however, the calculated Qf values were higher than the measured ones because the measured Qf value at microwave frequency included extrinsic loss factor, such as

Table 2
Measured and calculated properties of $BiNbO_4$ specimens

Sintering temperature (°C)	Measured		Calculated	
	K	Qf (GHz)	K	Qf (GHz)
1020	40.5	13690	42.0	15700
1030	44.4	1600	44.0	12500
1040	–	–	30.2	8900

Table 3
Microwave dielectric properties of $BiNbO_4$ specimens with CuV_2O_6

Sintering temperature (°C)	CuV_2O_6 (wt.%)	Phase	Density	K	Qf (GHz)	TCF (ppm/°C)
1000	0.01	Orthorhombic	6.224	–	–	–
	0.03	Orthorhombic	7.132	44.9	16100	−3.4
	0.05	Orthorhombic	7.161	45.5	13600	−2.7
1050	0.01	Triclinic	6.208	–	–	–
	0.03	Triclinic	6.983	34.9	9870	−35.7
	0.05	Triclinic	6.875	–	–	–

Table 4
Octahedral distortion of $BiNbO_4$ specimens

	Orthorhombic	Triclinic	
		(1)	(2)
Individual bond length (R_i)	1.8470	1.8000	1.8000
	1.8470	1.8100	1.8700
	1.8470	1.9100	1.9000
	1.8470	1.9800	1.9700
	1.9880	2.2400	2.1000
	1.9880	2.3100	2.2300
Average bond length (R_m)	1.8940	2.0083	1.9783
$(R_i - R_m)^2/R_m^2$	0.0006	0.0108	0.0081
	0.0006	0.0098	0.0030
	0.0006	0.0024	0.0016
	0.0006	0.0002	0.0000
	0.0025	0.0133	0.0038
	0.0025	0.0226	0.0162
Sum	0.0074	0.0590	0.0327
Δ ($\times 10^4$)	12.3	98.3	54.5
Average Δ ($\times 10^4$)	12.3	76.4	

porosity and the grain boundary. For the specimens sintered at 1040 °C, the microwave dielectric properties of the specimens could not be measured due to their poor sinterability, while the calculated dielectric properties could be obtained.

In order to evaluate the microwave dielectric properties of triclinic phase, the orthorhombic and/or the triclinic single phase of $BiNbO_4$ were prepared by the calcination at 1000 °C and/or 1100 °C for 6 h, respectively. The sintering aid, CuV_2O_6 was added to each calcined powders from 0.01 to 0.05 wt.%. The pressed specimens with CuV_2O_6 were sintered at 1000 °C for 3 h for the orthorhombic single phase and/or were sintered at 1050 °C for 3 h for the triclinic single phase of $BiNbO_4$.

The microwave dielectric properties of $BiNbO_4$ with CuV_2O_6 are shown in Table 3. For the sintered specimens with 0.03 wt.% CuV_2O_6, the dielectric constant and the Qf value of triclinic phase was lower than that of orthorhombic phase. For the temperature coefficient of resonant frequency (TCF), the specimens with 0.03 wt.% CuV_2O_6 showed −35.7 ppm/°C for triclinic phase, and −3.4 ppm/°C for orthorhombic phase. The decrease of TCF with phase transition could be explained by the change of crystal structure from orthorhombic to triclinic.

According to the Subramanian and Calabrese,[18] the orthorhombic $BiNbO_4$ has a [Nb–O] octahedron with two kinds of Nb–O interatomic distances; 1.847 and 1.988 Å, while Keve and Skapsi reported[19] that the triclinic $BiNbO_4$ has two kinds of [Nb–O] octahedra with a different Nb–O interatomic distances: (1) 1.80, 1.81, 1.91, 198, 2.24, 2.31 Å; and (2) 1.80, 1.87, 1.90, 197, 2.10, 2.23 Å. On the other hand, it has been reported[20] that the distortion of oxygen octahedron could be evaluated by Eq. (1).

Table 5
Bond valence of Nb–O octahedral in $BaNbO_4$ specimens

Nb–O	Nb–O bond						V_{Nb-O}	
	1	2	3	4	5	6		
Orthorhombic $BiNbO_4$								
R_0	1.911							
R_{NbO}	2.324	2.324	2.122	2.122	2.740	2.740	5.025	
$(R_0 - R_{NbO})/b$	−0.21	−0.21	−0.67	−0.67	0.173	0.173		
$\exp\{(R_0 - R_{NbO})/b\}$	0.812	0.812	0.512	0.512	1.189	1.189		
Triclinic $BiNbO_4$								
Octahedron 1								
R_0	1.911						5.247	5.310
R_{NbO}	1.800	1.810	1.910	1.980	2.240	2.310		
$(R_0 - R_{NbO})/b$	0.3	0.273	0.003	−0.19	−0.89	−1.08		
$\exp\{(R_0 - R_{NbO})/b\}$	1.350	1.314	1.003	0.830	0.411	0.340		
Octahedron 2								
R_0	1.911						5.372	
R_{NbO}	1.800	1.870	1.900	1.970	2.100	2.230		
$(R_0 - R_{NbO})/b$	0.300	0.111	0.030	−0.16	−0.51	−0.86		
$\exp\{(R_0 - R_{NbO})/b\}$	1.350	1.117	1.030	0.853	0.600	0.422		

Table 4 shows the [Nb–O] octahedral distortion of the orthorhombic and the triclinic $BiNbO_4$. The [Nb–O] octahedral distortion was increased by the phase transition from orthorhombic to triclinic, which in turn, the bond strain was increased due to the octahedral distortion. The increase of bond strain due to the phase transition could also be confirmed by the increase of Nb–O bond valence ($V_{Nb–O}$), as shown in Table 5. These results are agreed with the report[23] that the restoring force to the tilting recovers increased and *TCF* decreased with the increase of B-site bond valence in ABO_3 perovskite compounds. Therefore, the decrease of *TCF* with phase transition of $BiNbO_4$ in this study was due to the increase of bond strain resulting from the [Nb–O] octahedral distortion of $BiNbO_4$.

4. Conclusions

The phase transition of $BiNbO_4$ from orthorhombic to triclinic phase was observed for the specimens sintered at 1040 °C for 3 h. From the ICP data, the ratios of Bi to Nb were not changed with sintering temperature remarkably. With the increase of sintering temperature, *K* and *Qf* value of the specimens increased with sintering temperature up to 1030 and 1020 °C, respectively, and then decreased remarkably.

For the sintered specimens with 0.03 wt.% CuV_2O_6, the dielectric constant and the *Qf* value of triclinic phase was lower than that of orthorhombic phase, and the temperature coefficient of resonant frequency (*TCF*) was changed from −35.7 ppm/°C for triclinic phase to −3.4 ppm/°C for orthorhombic phase. These results are due to the increase of the octahedral distortion of $BiNbO_4$ with phase transition from orthorhombic to triclinic phase, which in turn, the Nb–O bond strain and bond valence ($V_{Nb–O}$) were increased.

Acknowledgement

This work was supported by Grant No. R01-2001-000-00262-0 from the Korea Science and Engineering Foundation.

References

1. Ishizaki, S. T., Fujita, M., Kagata, H., Uwano, T. and Miyake, H., A very small dielectric planar filter for portable telephones. *IEEE Trans. Microw. Theor. Tech.*, 1994, **MTT-42**, 2017–2022.
2. Ishizaki, T., Uwano, T., Kagata, H., Miyake, H. and Fujita, M., A small laminated planar filter for use in compact portable telephones. *Microwave*, 1995, **38**, 106–120.
3. Wakino, K., Minai, K. and Tamura, H., Microwave characteristics of (Zr,Sn)TiO_4 and BaO–PbO–Nd_2O_3–TiO_2 dielectric resonators. *J. Am. Ceram. Soc.*, 1994, **67**, 278–281.
4. Liu, D., Liu, Y., Huang, S. Q. and Yao, X., Phase structure and dielectric properties of Bi_2O_3–ZnO–Nb_2O_5-based dielectric ceramics. *J. Am. Ceram. Soc.*, 1993, **76**, 2129–2132.
5. Ling, H. C., Yan, M. F. and Rhodes, W. W., High dielectric constant and small temperature coefficient bismuth-based dielectric compositions. *J. Mater. Res.*, 1990, **5**, 1752–1756.
6. Kagata, H., Inoue, T., Kato, J. and Kameyama, I., Low-fire bismuth dielectric ceramics for microwave use. *Jpn. J. Appl. Phys.*, 1992, **31**(9B (Part I)), 3152–3155.
7. Choi, W. and Kim, K. Y., Effects of Nd_2O_3 on the microwave dielectric properties of $BiNbO_4$ ceramics. *J. Mater. Res.*, 1998, **12**, 2945–2949.
8. Tzou, W. C., Yang, C. F., Chen, Y. C. and Cheng, P. S., Microwave dielectric characteristics of $(Bi_{1-x}Sm_x)NbO_4$ ceramics. *Ceram. Inter.*, 2002, **28**, 105–110.
9. Huang, C. L., Weng, M. H. and Wu, C. C., The microwave dielectric properties and the microstructures of La_2O_3-modified $BiNbO_4$ ceramics. *Jpn. J. Appl. Phys.*, 2000, **39**(6A (Part I)), 3506–3510.
10. Weng, M. H. and Huang, C. L., The microwave dielectric properties and the microstructures of Bi(Nb,Ta)O_4 ceramics. *Jpn. J. Appl. Phys.*, 1999, **38**, 5949–5952.
11. Wang, N., Zhao, M. Y., Li, W. and Yin, Z. W., The sintering behavior and microwave dielectric properties of Bi(Nb,Sb)O_4 ceramics. *Ceram. Inter.*, 2004, **30**, 1017–1022.
12. Huang, C. L., Weng, M. H. and Yu, C. C., Low firable $BiNbO_4$ based microwave dielectric ceramics. *Ceram. Inter.*, 2001, **27**(3), 343–350.
13. Tzou, W. C., Yang, C. F., Chen, Y. C. and Cheng, P. S., Improvement in the sintering and microwave properties of $BiNbO_4$ microwave ceramics by V_2O_5 addition. *J. Eur. Ceram. Soc.*, 2000, **20**, 991–996.
14. Wakino, K., Murata, M. and Tamura, H., Far infrared reflection spectra of Ba(Zn,Ta)O_3–$BaZrO_3$ dielectric resonator material. *J. Am. Ceram. Soc.*, 1986, **69**, 34–37.
15. Brown, I. D. and Altermatt, D., Bond valance parameters obtained from a systemic analysis of the inorganic crystal structure database. *Acta. Cryst.*, 1985, **B41**, 244–247.
16. Hakki, B. W. and Coleman, P. D., A dielectric method of measuring inductive capacitance in the millimeter range. *IEEE Trans. Microw. Theory Tech.*, 1960, **8**, 402–410.
17. Nishikawa, T., Wakino, K., Tamura, H., Tanaka, H. and Ishikawa, Y., Precise measurement method for temperature coefficient of microwave dielectric resonator material. *IEEE MTT-S Int. Microw. Symp. Dig.*, 1987, 277–280.
18. Subramanian, M. A. and Calabrese, J. C., Crystal structure of the low temperature form of bismuth niobium oxide. *Mater. Res. Bull.*, 1993, **28**, 523–529.
19. Keve, E. T. and Skapski, A. C., The crystal structure of triclinic b-$BiNbO_4$. *J. Solid State Chem.*, 1973, **8**, 159.
20. Shannonn, R. D., Revised effective ionic radii and systematic studies of interatomic distance in hallides and chalcogenides. *Acta. Cryst.*, 1976, **A32**, 751.
21. Mhaisalkar, S. G., Readey, D. W., Akbar, S. A., Dutta, P. K., Sumnar, M. J. and Rokhlin, R., Infrared reflectance spectra of doped $BaTi_4O_9$. *J. Solid State Chem.*, 1991, **195**, 275–282.
22. Spitzer, W. G., Miller, R. C., Kleinman, D. A. and Howarth, L. E., Far-infrared dielectric dispersion in $BaTiO_3$, $SrTiO_3$, and TiO_2. *Phys. Rev.*, 1962, **126**(5), 1710–1721.
23. Kim, E. S. and Yoon, K. H., Microwave dielectric properties of $(1-x)CaTiO_3$–$xLi_{1/2}Sm_{1/2}TiO_3$ ceramics. *J. Eur. Ceram. Soc.*, 2003, **23**, 2397–2401.